

Comparative molecular field analysis of flavonoid inhibitors of the PIM-1 kinase

Sheldon Holder,^{a,b,c} Michael Lilly^{a,b,c} and Milton L. Brown^{d,*}

^aCenter for Molecular Biology & Gene Therapy, Loma Linda University School of Medicine, Loma Linda, CA 92354, USA

^bDepartment of Biochemistry and Microbiology, Loma Linda University School of Medicine, Loma Linda, CA 92354, USA

^cDepartment of Medicine, Loma Linda University School of Medicine, Loma Linda, CA 92354, USA

^dGeorgetown University Medical Center, Department of Oncology, Washington, DC 20057, USA

Received 24 December 2006; revised 23 May 2007; accepted 12 June 2007

Available online 14 June 2007

Abstract—The PIM-1 protein, the product of the *pim-1* oncogene, is a serine/threonine kinase. Dysregulation of the PIM-1 kinase has been implicated in the development of human malignancies including lymphomas, leukemias, and prostate cancer. Comparative molecular field analysis (CoMFA) is a 3-D QSAR technique that has been widely used, with notable success, to correlate biological activity with the steric and electrostatic properties of ligands. We have used a set of 15 flavonoid inhibitors of the PIM-1 kinase, aligned de novo by common substructure, to generate a CoMFA model for the purpose of elucidating the steric and electrostatic properties involved in flavonoid binding to the PIM-1 kinase. Partial least squares correlation between observed and predicted inhibitor potency (expressed as $-\log IC_{50}$), using a non-cross-validated partial least squares analysis, generated a non-cross-validated $q^2 = 0.805$ for the training set ($n = 15$) of flavonoids. The CoMFA generated steric map indicated that the PIM-1-binding site was sterically hindered, leading to more efficient binding of planar molecules over (*R*) or (*S*) compounds. The electrostatic map identified that positive charges near the flavonoid atom C8 and negative charges near C4' increased flavonoid binding. The CoMFA model accurately predicted the potency of a test set of flavonoids ($n = 6$), generating a correlation between observed and predicted potency of $q^2 = 0.825$. CoMFA models generated from additional alignment rules, which were guided by co-crystal structure ligand orientations, did not improve the correlative value of the model. Superimposing the PIM-1 kinase crystal structure onto the CoMFA contours validated the steric and electrostatic maps, elucidating the amino acid residues that potentially contribute to the CoMFA fields. Thus we have generated the first predictive model that may be used for the rational design of small-molecule inhibitors of the PIM-1 kinase.

© 2007 Published by Elsevier Ltd.

1. Introduction

The PIM-1 protein is a serine/threonine kinase^{1–3} that has been shown to be involved in the regulation of cell survival, differentiation, proliferation, and tumorigenesis (for review, see Refs. 4,5). The *pim-1* gene was first identified as a preferential proviral insertion site of Moloney Murine Leukemia Virus in virally induced T-cell lymphomas in mice.⁶ In humans, *pim-1* is expressed in normal lymphoid tissues (bone marrow, spleen, thymus, and lymph nodes), testis, and circulating myeloid cells.^{7,8} Although its specific role is not known, the PIM-1 kinase has been shown to be an integral part

of growth factor signaling.^{9–17} Additionally, the PIM-1 kinase is involved in regulating the activity of phosphatases^{18,19} and transcription factors,^{20,21} and has been shown to phosphorylate heterochromatin protein 1 (HP1),²² Pim-1 associated protein 1 (PAP-1),²³ and the nuclear mitotic apparatus protein (NuMA),²⁴ all nuclear proteins involved in chromatin remodeling. The PIM-1 kinase has also been shown to phosphorylate and inactivate the pro-apoptotic protein BAD.^{25,26}

While the PIM-1 kinase is involved in numerous signaling events in normal cells, *pim-1* knockout mice only exhibit a minimal phenotype. The near normal phenotype of these mice is attributed to functional compensation by other members of the PIM family of kinases, namely PIM-2 and PIM-3.²⁷ Not surprisingly, hematopoietic cells taken from triple knockout mice devoid of PIM-1, PIM-2, and PIM-3 demonstrated to have an

Keywords: Pim-1; Comparative molecular field analysis (CoMFA); Flavonoids; Kinase inhibitors.

* Corresponding author. Tel.: +1 202 687 8603; fax: +1 202 687 7659; e-mail: mb544@georgetown.edu

impaired response to growth factors.²⁸ While the absence of *pim-1* showed minimal adverse effects in mice, over-expression of *pim-1* has been shown to have significant effects on cell survival. In vitro studies reveal that enforced expression of *pim-1* caused increased cellular proliferation, decreased apoptosis and cell death, increased cell survival,²⁹ and protection from toxin-induced cell death³⁰ in the murine bone marrow FDCP1 cell line. Enforced expression of human *pim-1* in FDCP1 cells also resulted in IL-3-independent cell survival.³¹ Furthermore, *pim-1* has been shown to cooperate with both *c-myc* and *N-myc* in hematopoietic oncogenesis⁸ and significant over-expression of *pim-1* has been demonstrated in clinical cases of lymphoma,^{32,33} leukemia,⁷ and prostate cancer.^{34,35}

Comparative molecular field analysis (CoMFA) is a three-dimensional quantitative molecular modeling technique used to study relationships between ligand structure (steric and electrostatic properties) and biological activity. The final validated model can be used for the design of novel ligands and to predict the functional activity of those ligands before synthesis.

In addition to its successful use to evaluate the properties of the binding sites of kinase-specific inhibitors,^{36–38} the CoMFA methodology has shown utility in evaluating the ligand-binding sites of numerous receptors,^{39–54} calcium channels,⁵⁵ chromosome p450 enzymes,^{56–60} human immunodeficiency virus-1 integrase,⁶¹ and β -tubulin.⁶² In each case the CoMFA models demonstrated a strong correlation between predicted and experimental ligand activity.

We have constructed CoMFA models, aligned with and without crystal structure guidance, for flavonoid ligands of the PIM-1 kinase using a training set of 15 flavonoid probes for which we have determined the inhibitory potency against the PIM-1 kinase. Here we describe the electrostatic and steric properties of the CoMFA model. We demonstrated its utility as a predictive model of flavonoid potency using a test set of six flavonoids that were not included in the training set. We also validated the model by overlay with a PIM-1 kinase crystal structure to elucidate the amino acid residues that may provide an explanation of the CoMFA contours.

2. Results

Simple correlations between PIM-1 kinase inhibition and flavonoid $\log P$ (Fig. 1) or molecule dipole (Fig. 2) resulted in poor correlations. This suggested that other parameters are important for kinase inhibition.

Hence we generated CoMFA models of flavonoid inhibitors of the PIM-1 kinase. The structures and corresponding $-\log IC_{50}$ values for the training set of flavonoids are presented in Table 1. A cross-validated partial least squares analysis determined the optimum number of components for use in non-cross-validated analysis to be 2 (Table 2).

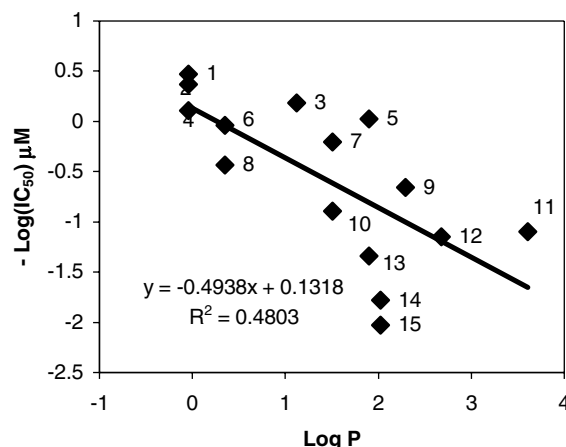


Figure 1. Predictive value of $\log P$ versus inhibitor potency for the training set.

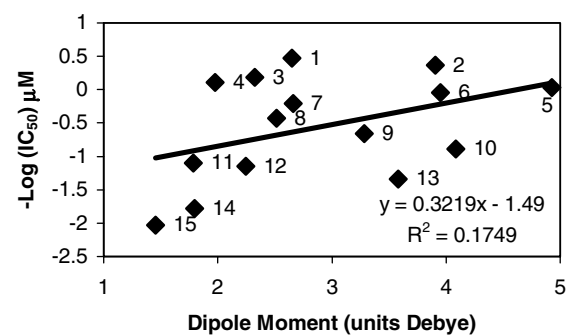


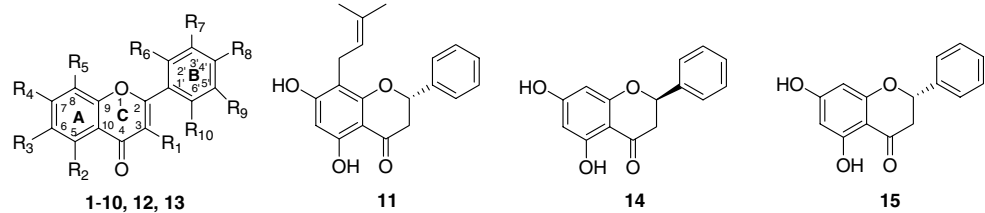
Figure 2. Predictive value of dipole moment versus inhibitor potency for the training set.

Using the alignment rule for model I (Fig. 3), a non-cross-validated partial least squares regression analysis of potency, expressed as $-\log IC_{50}$, and CoMFA descriptors generated a CoMFA model with $q^2 = 0.805$ for the training set (see Table 1 and Fig. 4a). The CoMFA model provided an improved correlation to flavonoid potency compared with $\log P$ ($R^2 = 0.4803$) or dipole moment ($R^2 = 0.1749$) for the same set of data.

We validated the CoMFA model by determining how accurately it could predict the IC_{50} values of a test set of compounds (flavonoids not included in the training set; Table 3). We compared the CoMFA predicted $-\log IC_{50}$ with the experimental $-\log IC_{50}$ for each flavonoid in the test set. The model showed a strong correlation between predicted $-\log IC_{50}$ and experimental $-\log IC_{50}$ with a correlation coefficient of $R^2 = 0.829$ (Fig. 4b). These data demonstrated that the CoMFA model could successfully predict the potency of flavonoid inhibitors of the PIM-1 kinase not present in the training set.

The steric and electrostatic contributions to the model were determined to be 0.626 and 0.374, respectively, and are represented graphically in Figure 5. For electrostatic contributions the model predicts that increased binding will result by placing more negative charge near the flavonoid C4' position and more positive charges near C8. For steric contributions the model predicts that

Table 1. Structures and non-cross-validated PLS analysis for the training set using multiple alignments

										
Compound	R ₁	R ₂	R ₃	R ₄	R ₅	R ₆	R ₇	R ₈	R ₉	R ₁₀
1 (quercetagenin)	OH	OH	OH	OH	H	H	OH	OH	H	H
2 (gossypetin)	OH	OH	H	OH	OH	H	OH	OH	H	H
3	H	OH	H	OH	H	H	OH	OH	OH	H
4 (myricetin)	OH	OH	H	OH	H	H	OH	OH	OH	H
5 (apigenin)	H	OH	H	OH	H	H	H	OH	H	H
6 (quercetin)	OH	OH	H	OH	H	H	OH	OH	H	H
7 (luteolin)	H	OH	H	OH	H	H	OH	OH	H	H
8 (morin)	OH	OH	H	OH	H	OH	H	OH	H	H
9	H	H	H	OH	H	H	OH	H	H	H
10	H	H	H	OH	H	H	OH	OH	OH	H
12	H	H	H	OH	H	H	H	H	H	H
13	H	H	H	OH	OH	H	H	OH	H	H

Compound	Model I –logIC ₅₀ (μM)			Model II –logIC ₅₀ (μM)		Model III –logIC ₅₀ (μM)	
	Obsd	Pred ^a	Res	Pred ^a	Res	Pred ^a	Res
1	0.47	0.20	0.27	0.28	0.19	0.32	0.15
2	0.37	0.21	0.16	0.31	0.06	0.34	0.03
3	0.19	0.23	–0.05	0.29	–0.11	0.02	0.17
4	0.11	0.28	–0.18	–0.10	0.21	0.005	0.1
5	0.03	0.09	–0.06	0.19	–0.17	0.21	–0.18
6	–0.04	–0.25	0.21	–0.29	0.24	–0.39	0.35
7	–0.20	–0.12	–0.08	–0.16	–0.04	–0.19	–0.01
8	–0.43	–0.78	0.35	–0.82	0.39	–0.80	0.37
9	–0.66	–0.98	0.33	–0.91	0.25	–0.88	0.22
10	–0.89	–0.86	–0.03	–0.84	–0.05	–0.67	–0.23
11	–1.10	–1.76	0.67	–1.77	0.68	–1.82	0.72
12	–1.15	–0.98	–0.17	–0.91	–0.23	–0.89	–0.26
13	–1.34	–0.89	–0.46	–0.89	–0.45	–0.86	–0.48
14-(R)	–1.78	–1.05	–0.73	–1.03	–0.75	–1.01	–0.77
15-(S)	–2.03	–1.78	–0.25	–1.81	–0.22	–1.84	–0.19

Obsd, observed value; pred, predicted value; res, residual.

^a Generated from CoMFA non-cross-validated run (see Section 4). $R^2 = 0.805$ (model I), 0.800 (model II), 0.781 (model III).**Table 2.** Cross-validated partial least squares analysis using multiple alignments

Components	Model I		Model II		Model III	
	s	R ²	s	R ²	s	R ²
1	0.682	0.303	0.686	0.296	0.711	0.244
2	0.610	0.487	0.630	0.452	0.654	0.409
3	0.679	0.416	0.669	0.433	0.696	0.386
4	0.691	0.450	0.731	0.385	0.728	0.390
5	0.778	0.374	0.760	0.401	0.787	0.358
6	0.861	0.318	0.819	0.382	0.864	0.312

s, standard error for the estimate of $-\log IC_{50}$; R^2 , correlation coefficient. Optimum number of components for model I is 2 ($R^2 = 0.487$), model II is 2 ($R^2 = 0.452$), model III is 2 ($R^2 = 0.409$).

adding bulk near the C3' and C6' positions will improve binding.

We examined the interactions of the most potent PIM-1 antagonist, quercetagenin ($IC_{50} = 0.34 \mu M$), and those of the least potent flavonoid, compound **15** ($IC_{50} =$

$107 \mu M$), with the steric and electrostatic contours of the model. The model elucidates at least one reason for the dramatic differences in potency between these two flavonoid compounds. As illustrated in Figure 6, quercetagenin lies almost completely flat within the contours. In this position the C3' and C4' hydroxyl groups on the

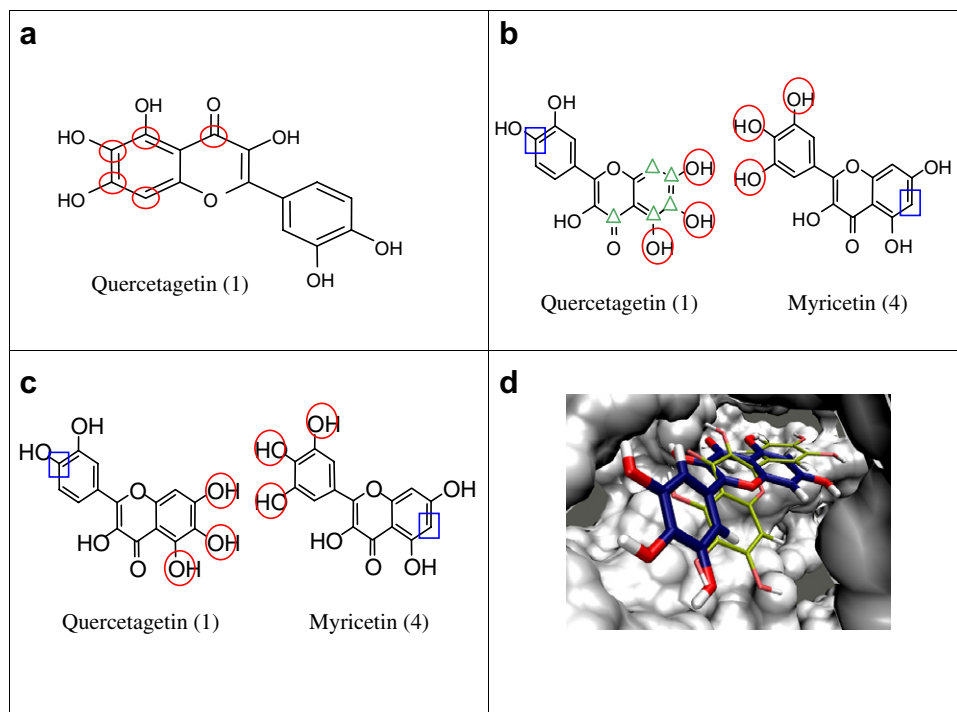


Figure 3. CoMFA model alignment rules. (a) In model I compounds **2–21** were aligned by overlapping atoms indicated by red circles. (b) In model II myricetin was aligned to quercetagenin according to their respective poses within the co-crystallized PIM-1 structures. To achieve this alignment the protein crystal structure backbones of PIM-1/quercetagenin and PIM-1/myricetin were aligned. The relationship of the quercetagenin pose to the myricetin pose is illustrated by overlap of atoms indicated by blue squares and red circles. Compounds **2, 3, 5–21** were aligned to quercetagenin as in model I (indicated by green triangles). (c) In model III compounds **3** and **10** were aligned to the co-crystallized pose of myricetin. Compounds **2, 5–9, 11–21** were aligned to the co-crystallized pose of quercetagenin. (d) The crystal poses of quercetagenin (blue) and myricetin (green) in the PIM-1 ATP-binding pocket.

B ring are directed toward the area revealed by the model as favorable for negative charges (red contours). In contrast, compound **15** has a chiral center at the C2 position and does not lie flat within the contours (because of the sp^3 hybridization). The B ring of this flavonoid is positioned deep within a region where the model predicted less bulk would improve binding (yellow contour). Hence the model elucidates the steric interactions that make compound **15** a poor PIM-1 kinase inhibitor, that is, the position of the B ring produces steric hindrances that discourage flavonoid binding.

We sought to further validate the CoMFA model by comparing the steric and electrostatic contours of the model with a PIM-1 kinase crystal structure. We have previously reported the crystal structure of the PIM-1 kinase in complex with quercetagenin.⁶³ We superimposed the quercetagenin in the PIM-1 co-crystal structure onto the quercetagenin in the CoMFA training set and examined the amino acid residues involved in flavonoid binding. In the areas where the model predicts improved binding by the addition of more positive charges, there are potential interactions with negatively charged acidic side chains (Glu¹²¹, Asp¹²⁶, Asp¹³¹, Glu¹⁷¹). Similarly, the electrostatic contour favoring negative charges envelops the positively charged side chain of Lys⁶⁷ (Fig. 6a).

The steric fields were also confirmed by the PIM-1 kinase crystal structure. The bulky side chains of Val⁵², Ala⁶⁵, and Leu¹²⁰ sterically hinder large groups in the

region identified in the crystal structure that corresponds to regions in the CoMFA model where reduced bulk will improve binding. The model also identified a solvent exposed area near C7 as a region where reduced bulk would improve binding. Additionally, the side chain of Phe⁴⁹ and those of Ile¹⁰⁴ and Ile¹⁸⁵ form two hydrophobic pockets. The model accurately identified both of these pockets as regions where the addition of bulk would improve binding (Fig. 6b). Hence, a comparison of the electrostatic and steric CoMFA fields with the PIM-1 kinase crystal structure validates the striking accuracy of this CoMFA model of the PIM-1 kinase.

To address the finding that flavonoids bind to the PIM-1 kinase in at least two different orientations we created additional CoMFA models using alternate alignment rules (Fig. 3). Model II, in which myricetin was aligned in the training set of compounds according to its crystal pose rather than by superimposition onto quercetagenin over their common substructure, showed no improvement over model I to predict the potencies of the test set of compounds (Fig. 4). Similarly, model III, in which myricetin and compounds **3** and **10** were aligned in the training set according to the crystal pose of myricetin, showed no improvement over model I in predicting the potencies of the test set compounds (Fig. 4).

In light of the sterically restricted nature of the PIM-1 kinase ATP binding site we evaluated the relationship between volume and potency for flavonoid inhibitors

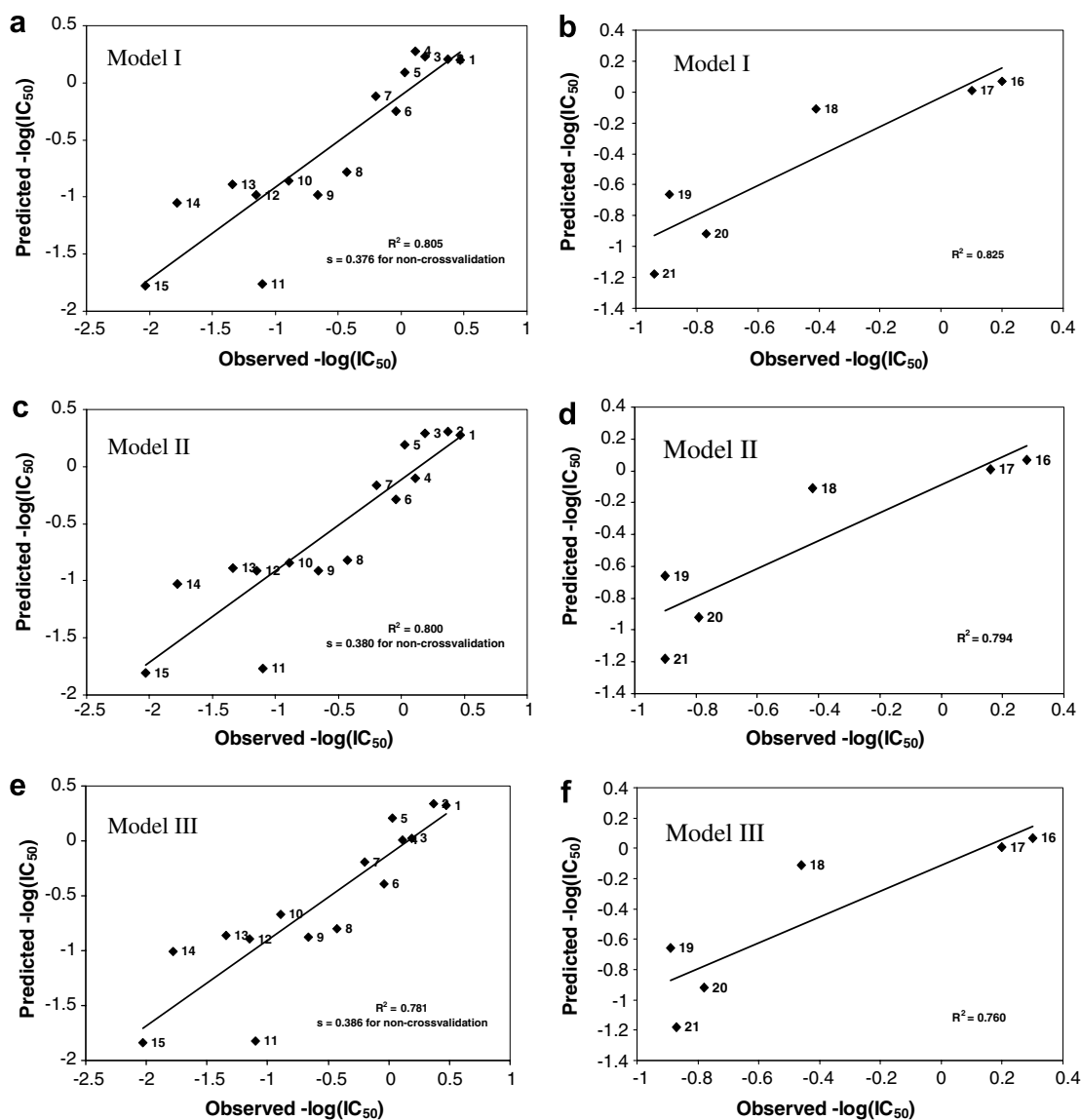


Figure 4. Training and test set analyses using multiple alignment rules. The correlation between predicted and observed potencies for the training set using CoMFA models I, II, and III (a, c, e, respectively) is shown. The test set results for models I, II, and III are presented in panels b, d, and f, respectively.

of the PIM-1 kinase. **Figure 7** demonstrates what appears to be an optimum volume near 218 \AA^3 (the volume of quercetagenin) for flavonoid antagonists of PIM-1. Flavonoids with volumes larger or smaller than 218 \AA^3 are progressively worse inhibitors of the PIM-1 kinase.

3. Discussion

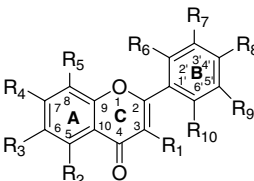
Here we have described the generation of the first CoMFA model for PIM-1 kinase ligands using flavonoid probes. Sixty-three percent of the contributions to the model were steric, while only 37% were electrostatic, suggesting that flavonoid binding to the PIM-1 kinase is influenced predominantly by steric factors rather than by electrostatic factors.

The steric contours reveal that the PIM-1 kinase ATP-binding site is sterically hindered above and below the

plane of the bound flavonoid. It is likely that the planar conformation of the flavone class of compounds is what allows them to fit well into the sterically restricted space within the PIM-1 kinase ATP-binding site. In contrast, (*R*)- and (*S*)-flavanones (compounds **11**, **14**, and **15**), which have a chiral carbon at the C2 position, are inferior PIM-1 kinase antagonists compared to the flavones (see **Fig. 6** and **Table 1**). Our model was able to predict the relative order in regard to enantioselective inhibition ($R > S$) of compounds **14** and **15**. It appears that a planar conformation is advantageous for inhibition and presumably would not be limited to the flavonoid class of compounds. It is more likely that this favorable characteristic will be found in small-molecule inhibitors of the PIM-1 kinase as a group.

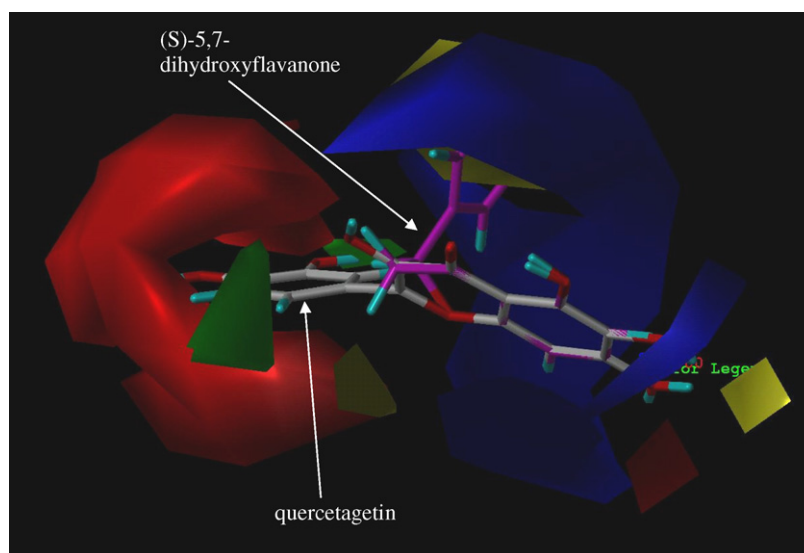
As demonstrated in **Figure 7**, the volume of the ligand also appears to play a role in the potency of flavonoid compounds as PIM-1 kinase antagonists. This feature

Table 3. Observed and predicted potencies for the test set using multiple alignments

										
16-21										
Compound	R ₁	R ₂	R ₃	R ₄	R ₅	R ₆	R ₇	R ₈	R ₉	R ₁₀
16 (fisetin)	OH	H	H	OH	H	H	OH	OH	H	H
17	OH	H	H	OH	H	H	H	OH	H	H
18 (kaempferol)	OH	OH	H	OH	H	H	H	OH	H	H
19	OH	H	H	OH	H	H	H	H	H	H
20	OH	H	OH	H	H	OH	H	OH	H	H
21	H	OH	H	OH	H	H	H	H	H	H

Compound	Model I –log IC ₅₀ (μM)			Model II –log IC ₅₀ (μM)		Model III –log IC ₅₀ (μM)	
	–log IC ₅₀ (μM)			–log IC ₅₀ (μM)		–log IC ₅₀ (μM)	
	Obsd	Pred ^a	Res	Pred ^a	Res	Pred ^a	Res
16 (fisetin)	0.07	0.20	–0.13	0.28	–0.21	0.30	–0.23
17	0.01	0.10	–0.09	0.16	–0.15	0.20	–0.19
18 (kaempferol)	–0.11	–0.41	0.30	–0.42	0.31	–0.46	0.35
19	–0.66	–0.89	0.23	–0.90	0.24	–0.89	0.23
20	–0.92	–0.77	–0.15	–0.79	–0.13	–0.78	–0.14
21	–1.18	–0.94	–0.24	–0.90	–0.28	–0.87	–0.31

Obsd, observed value; pred, predicted value; res, residual.

^a Generated from CoMFA non-cross-validated run (see Section 4).**Figure 5.** Comparison of the most and least potent flavonoid inhibitors of the PIM-1 kinase within the contours of the CoMFA model. Quercetagetin, the most potent inhibitor, is pictured in gray. (S)-5,7-Dihydroxyflavanone (**15**), the poorest inhibitor, is pictured in purple. For the electrostatic contours increased binding is predicted by placing more positive (+) charges near blue areas and more negative (–) charges near red areas. The steric contours predict increased binding by placing more bulk near green areas and less bulk near yellow areas.

is related to the sterically restricted nature of the binding site. It appears that the potency of a flavonoid is reduced when the volume of the flavonoid is too small to adequately fill the ATP-binding pocket. Similarly, if the volume of the flavonoid is too large the restrictive nature of the binding pocket results in reduced efficiency of binding and inferior potency. A volume approaching 218 Å³, the volume of quercetagetin, appears near optimal for flavonoid inhibitors of the PIM-1 kinase.

The CoMFA model generated a superior correlation to observed flavonoid potency than simple correlation to either log *P* or dipole moment. It is important to note that the flavonoid potencies used to generate the CoMFA model were determined using a solid phase in vitro kinase assay. Because log *P* is a predictive measure of absorption, it is plausible that determining the flavonoid potencies using a cellular assay would improve the correlation between log *P* and observed flavonoid potency. Nonetheless, the utility of the CoMFA model

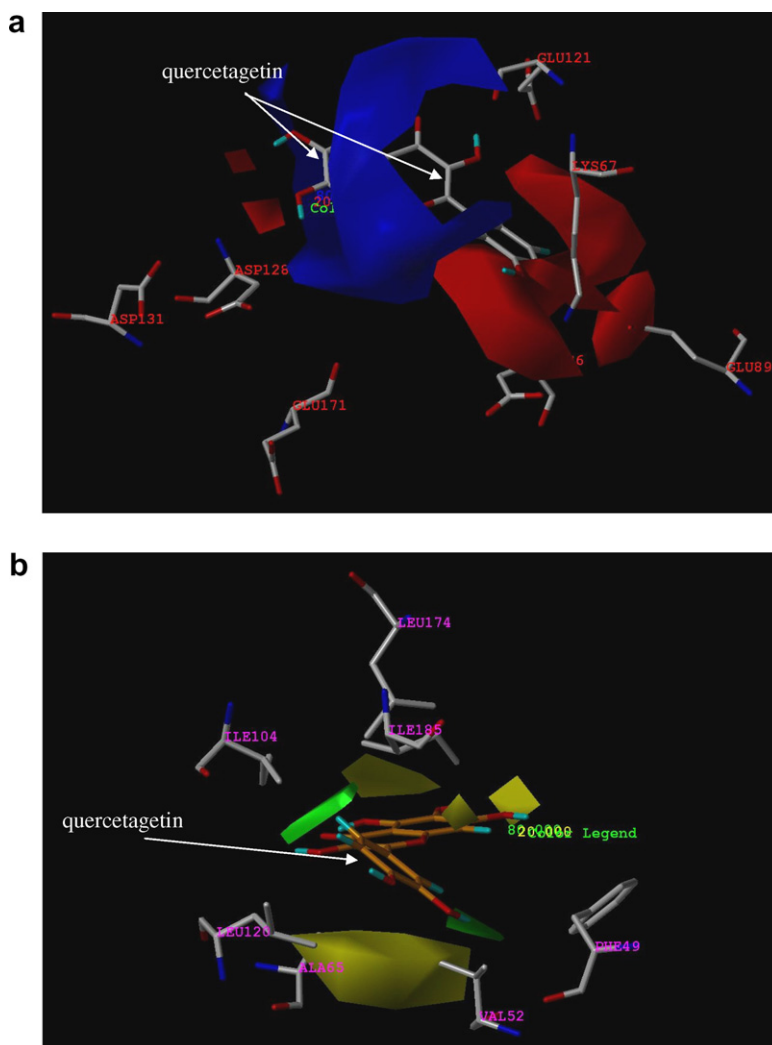


Figure 6. Characterization of the electrostatic and steric CoMFA fields with a superimposed PIM-1 kinase crystal structure. The crystal structure of the PIM-1 kinase in complex with quercetagetin is superimposed on the CoMFA fields using the positions of quercetagetin in the crystal and in the model. For clarity, only the amino acid residues contributing to the properties of a CoMFA contour are shown. The pictured flavonoid is the CoMFA model quercetagetin structure; to reduce visual clutter the PIM-1 crystal quercetagetin structure is not shown. (a) For the electrostatic contours increased binding is predicted by placing more positive (+) charges near blue areas and more negative (−) charges near red areas. (b) The steric contours predict increased binding by placing more bulk near green areas and less bulk near yellow areas.

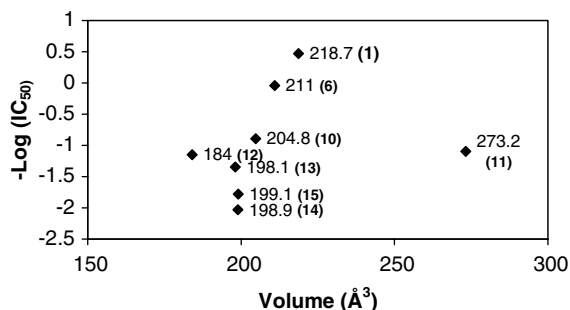


Figure 7. The volume of a flavonoid is related to its potency as an inhibitor of the PIM-1 kinase. The labels on the points represent the volume of each inhibitor. The bold numbers in parentheses identify the compound according to number as presented in Table 1.

as a predictive model of flavonoid potency was demonstrated by its ability to accurately predict the potency of the test set of flavonoids. These data suggest that the

model may be an effective tool for the in silico design and prediction of additional flavonoid inhibitors of the PIM-1 kinase. Further experiments will be conducted to determine the accuracy of using the model to determine the potency of small molecules that are not in the flavonoid class of compounds.

Additionally, the PIM-1 kinase crystal structure strongly supports the CoMFA model by providing reasonable rationale in regard to the amino acid residues that may contribute to the steric and electrostatic contours of the model. This type of analysis is fairly unique, as CoMFA models are usually employed when the structure of the enzyme or receptor protein is unknown. Similar types of analyses, where the contours of a CoMFA model for a protein were combined with a crystal structure of the enzyme, have been described.^{36,65–68} In each case, as in our case, the combination of the CoMFA contours with the enzyme structure elucidated

specific potential ligand–enzyme interactions and allowed for a more informed and predictive structure-based design effort.

Our analysis elucidated the three-dimensional contributions of specific amino acid residues to the steric and electrostatic properties of the PIM-1 kinase ATP-binding site. Results from these studies may provide invaluable information for the design of potent, selective inhibitors of the PIM-1 kinase.

Quercetagenin, quercetin, myricetin, and compound **3** share a common flavone scaffold and differ only in the number and positions of substituted hydroxyl groups onto the flavone backbone. Hence, our previous work demonstrating that these flavones do not all bind to the PIM-1 kinase in the same orientation was quite unexpected.⁶³

One of the weaknesses of CoMFA is the choice of the alignment rule. We show for the first time that caution must be used in aligning compounds even when they appear to have a common pharmacophore. The varied orientation of flavonoid binding to the PIM-1 kinase presented a potential limitation of the CoMFA model. The alignment rule used to create model I did not take into account the varied binding orientations (crystal poses) that could be present in the training set of flavonoids. However, alignment rules incorporating the crystal orientations of compounds in the training set (model II) did not improve the ability of the model to predict the potencies of the test set of compounds. This unique example provides strong evidence of the robustness in a correlated partial least squares in regard to establishing alignment rules.

It should be noted that, as a class of compounds, flavonoids have been shown to be inhibitors of other kinases in addition to the PIM-1 kinase. Protein kinase C⁶⁹ and protein kinase A⁷⁰ activity have been shown to be inhibited by flavonoids, with IC₅₀ values in the millimolar range. In contrast, flavonoids inhibit the PIM-1 kinase in the micromolar and submicromolar ranges.

Flavonoids are promiscuous compounds, in that their effect is not limited to the kinase class of enzymes. Flavonoids have been shown to induce mammalian topoisomerase II-dependent cleavage,⁷¹ and inhibit both mitochondrial NADH-oxidase⁷² and HIV-1 integrase.⁷³ Flavonoids have also been shown to inhibit soybean lipoxygenase and stimulate cyclooxygenase.⁷⁴ Gastric H⁺, K⁺-ATPase,⁷⁵ reverse transcriptases,⁷⁶ and DNA and RNA polymerases⁷⁶ are also inhibited by flavonoids. Common to many of these studies, regardless of the target enzyme, is the observation that the polyhydroxylated core plays a major role in the potency of flavonoids. This polyhydroxylation is also an important contributor to flavonoid promiscuity.

Comparing the hydroxylation patterns of quercetagenin and myricetin, as in Figure 3d, suggests that the trihydroxylated ring of the flavonoids is preferentially ori-

ented toward the same region when bound to the PIM-1 kinase. This general rule appears true whether the trihydroxylated ring is ring A (as in quercetagenin) or ring B (as in myricetin). An alignment rule based on this general rule would require compounds **3** and **10** to bind to the PIM-1 kinase in an orientation similar to myricetin, rather than quercetagenin. Such an alignment was employed for model III, with no improvement in the predictive value of the model.

The structure of myricetin is similar to that of quercetagenin, hence the two compounds share similar properties when aligned according to their common substructure (as in model I). Interestingly, when aligned according to their crystal orientations (as in models II and III) these two compounds still share similar spatial electrostatic and steric properties (see Fig. 3). This relationship likely contributes to the success of our model. Our findings demonstrate the utility of ligand-based methods, such as CoMFA, in elucidating structure activity relationships; particularly in cases where the binding orientations of ligands are unknown.

Thus the outcome of the three predictive models presented here demonstrates that with our training and test set of compounds CoMFA is sufficiently robust to provide predictive models despite the varied binding orientations of flavonoids to the PIM-1 kinase. The utility of our model has been demonstrated by its successful use to predict the potencies of the test set of flavonoids ($r^2 = 0.829$). Hence we present here the first predictive model that may be used for the rational design of small-molecule PIM-1 kinase inhibitors.

4. Methods

4.1. PIM-1 activity

The IC₅₀'s used in the CoMFA were recently reported for PIM-1 kinase activity.⁶³ These values were used without correction or normalization.

4.2. Molecular modeling

The octanol–water partition coefficient ($\log P$) for each flavonoid was calculated using Chemdraw version 6.0 (Cambridgesoft, Cambridge, MA). Molecular dipoles were calculated using MOPAC with default settings. The molecular volume (\AA^3) of each compound was calculated in SYBYL. The structures and IC₅₀ values of the set of flavonoids that form the training set are listed in Table 1. Table 3 lists the structures and IC₅₀ values for the flavonoids that form the test set.

The structures of all of the compounds were constructed in the BUILD/EDIT mode of SYBYL and energy-minimized by the conjugate gradient method using the Tripos force field⁶⁴ from a starting geometry of PIM-1 bound quercetagenin (2O3P). The flavonoids in the training and the test sets have a common double six-membered ring structure; hence atoms in this common sub-structure were used to create the alignment rule

for model I. All of the structures in the training set were aligned over the atoms C4, C5, C6, C7, and C8 of quercetagenin from the co-crystal structure with the PIM-1 kinase. Similarly, the flavonoids in the test set were also aligned over the atoms C4, C5, C6, C7, and C8. CoMFA, using default parameters, was calculated in the QSAR option of SYBYL 6.5. The CoMFA grid spacing was 2.0 Å in the *x*, *y*, and *z* directions, and the grid region was automatically generated by the CoMFA routine to encompass all molecules with an extension of 4.0 Å in each direction. An sp³ carbon (sterics) and a charge of +1.0 (electrostatics) were used as probes to generate the interaction energies at each lattice point. The default value of 30 kcal/mol was used as the maximum electrostatic and steric energy cutoff.

Using the training set of flavonoids, cross-validated and non-cross-validated partial least squares analyses (PLS) were performed within the SYBYL/QSAR routine. Cross-validation of the dependent column ($-\log IC_{50}$) and the CoMFA column was performed with 2.0 kcal/mol column filtering. Scaled by the CoMFA standard deviation, the cross-validated analysis generated an optimum number of components equal to 2 and $q^2 = 0.495$ (Table 2). PLS analysis with non-cross-validation, performed with two components, generated a standard error of estimate of 0.376, a probability ($R^2 = 0$) equal to 0.000, an *F* value ($n_1 = 2$, $n_2 = 12$) of 24.792, and a $q^2 = 0.805$ (Table 1). The relative steric (0.626) and electrostatic (0.374) contributions to the final model were contoured as the standard deviation multiplied by the coefficient at 80% for favored steric (contoured in green) and favored positive electrostatic (contoured in blue) effects and at 20% for disfavored steric (contoured in yellow) and favored negative electrostatic (contoured in red) effects, as shown in Figures 5–7.

On the basis of this analysis, the IC_{50} values of the test set of flavonoids were predicted and correlated to the observed IC_{50} values as determined in our laboratory (Table 3). The CoMFA contours were also compared with a PIM-1 crystal structure. A PIM-1 kinase crystal structure with bound quercetagenin (the most potent flavonoid inhibitor of the PIM-1 kinase among those we have assayed) was superimposed with atoms O1, C2, C3, C4, C5, C6, C7, and C8, onto the quercetagenin structure in the training set of compounds used to create the CoMFA model.

A crystal structure of myricetin in complex with the PIM-1 kinase revealed a surprisingly distinct and different binding orientation than quercetagenin.⁶³ Hence a second CoMFA alignment rule was employed (model II), in which myricetin was aligned to quercetagenin according to their crystal poses rather than by their common substructure as in model I. To accomplish this alignment the two crystal structures of the PIM-1 kinase in complex with quercetagenin and myricetin (RCSB Protein Data Bank codes 2O63, 2O64, respectively) were superimposed over their protein backbones. The two PIM-1 kinase structures are notably similar, with an RMSD over the complete protein backbone of only 0.58 Å. Quercetagenin and myricetin were extracted

from their respective PIM-1 kinase protein structures to achieve a ligand alignment and orientation based on the crystal poses. The remaining compounds in the training set were aligned to quercetagenin by their common substructure, as in model I.

Based on their respective hydroxylation patterns, compounds **3** and **10** were identified as likely candidates for binding to the PIM-1 kinase in a similar pose to myricetin, rather than that of quercetagenin (see the discussion section for a detailed explanation). Consequently a third alignment rule was employed (model III), where myricetin and compounds **3** and **10** were aligned in the crystal pose of myricetin, while the remaining compounds in the training set were aligned in the quercetagenin crystal pose.

Acknowledgments

We thank Ryan Bremer and Plexxikon, Inc. for making the co-crystal structures of PIM-1 bound to quercetagenin and myricetin available to us in advance of publication for use in this study. We thank the Drug Discovery Program at Georgetown Medical Center for financial support.

References and notes

1. Hoover, D.; Friedmann, M.; Reeves, R.; Magnuson, N. S. *J. Biol. Chem.* **1991**, *266*, 14018–14023.
2. Padma, R.; Nagarajan, L. *Cancer Res.* **1991**, *51*, 2486–2489.
3. Saris, C. J.; Domen, J.; Berns, A. *EMBO J.* **1991**, *10*, 655–664.
4. Wang, Z.; Bhattacharya, N.; Weaver, M.; Petersen, K.; Meyer, M.; Gapter, L.; Magnuson, N. S. *J. Vet. Sci.* **2001**, *2*, 167–179.
5. Bachmann, M.; Moroy, T. *Int. J. Biochem. Cell Biol.* **2005**, *37*, 726–730.
6. Cuypers, H. T.; Selten, G.; Quint, W.; Zijlstra, M.; Maandag, E. R.; Boelens, W.; van Wezenbeek, P.; Melief, C.; Berns, A. *Cell* **1984**, *37*, 41–150.
7. Amson, R.; Sigaux, F.; Przedborski, S.; Flandrin, G.; Givol, D.; Telerman, A. *Proc. Natl. Acad. Sci. U.S.A.* **1989**, *86*, 8857–8861.
8. van Lohuizen, M.; Verbeek, S.; Krimpenfort, P.; Domen, J.; Saris, C.; Radaszkiewicz, T.; Berns, A. *Cell* **1989**, *56*, 673–682.
9. Domen, J.; van der Lugt, N. M.; Laird, P. W.; Saris, C. J.; Berns, A. *Leukemia* **1993**, *7*(Suppl. 2), S108–S112.
10. Domen, J.; van der Lugt, N. M.; Laird, P. W.; Saris, C. J.; Clarke, A. R.; Hooper, M. L.; Berns, A. *Blood* **1993**, *82*, 1445–1452.
11. Lilly, M.; Le, T.; Holland, P.; Hendrickson, S. L. *Oncogene* **1992**, *7*, 727–732.
12. Miura, O.; Miura, Y.; Nakamura, N.; Quelle, F. W.; Witthuhn, B. A.; Ihle, J. N.; Aoki, N. *Blood* **1994**, *84*, 4135–4141.
13. Shirogane, T.; Fukada, T.; Muller, J. M.; Shima, D. T.; Hibi, M.; Hirano, T. *Immunity* **1999**, *11*, 709–719.
14. Wingett, D.; Long, A.; Kelleher, D.; Magnuson, N. S. *J. Immunol.* **1996**, *156*, 549–557.
15. Yip-Schneider, M. T.; Horie, M.; Broxmeyer, H. E. *Blood* **1995**, *85*, 3494–3502.

16. Zhu, N.; Ramirez, L. M.; Lee, R. L.; Magnuson, N. S.; Bishop, G. A.; Gold, M. R. *J. Immunol.* **2002**, *168*, 744–754.
17. Krumenacker, J. S.; Narang, V. S.; Buckley, D. J.; Buckley, A. R. *J. Neuroimmunol.* **2001**, *113*, 249–259.
18. Mochizuki, T.; Kitanaka, C.; Noguchi, K.; Muramatsu, T.; Asai, A.; Kuchino, Y. *J. Biol. Chem.* **1999**, *274*, 18659–18666.
19. Wang, Z.; Bhattacharya, N.; Meyer, M. K.; Seimiya, H.; Tsuruo, T.; Tonani, J. A.; Magnuson, N. S. *Arch. Biochem. Biophys.* **2001**, *390*, 9–18.
20. Rainio, E. M.; Sandholm, J.; Koskinen, P. J. *J. Immunol.* **2002**, *168*, 1524–1527.
21. Levenson, J. D.; Koskinen, P. J.; Orrico, F. C.; Rainio, E. M.; Jalkanen, K. J.; Dash, A. B.; Eisenman, R. N.; Ness, S. A. *Mol. Cell* **1998**, *2*, 417–425.
22. Koike, N.; Maita, H.; Taira, T.; Ariga, H.; Iguchi-Ariga, S. M. *FEBS Lett.* **2000**, *467*, 17–21.
23. Maita, H.; Harada, Y.; Nagakubo, D.; Kitaara, H.; Ikeda, M.; Tamai, K.; Takahashi, K.; Ariga, H.; Iguchi-Ariga, S. M. *Eur. J. Biochem.* **2000**, *267*, 5168–5178.
24. Bhattacharya, N.; Wang, Z.; Davitt, C.; McKenzie, I. F.; Xing, P. X.; Magnuson, N. S. *Chromosoma* **2002**, *111*, 80–95.
25. Yan, B.; Zemskova, M.; Holder, S.; Chin, V.; Kraft, A.; Koskinen, P. J.; Lilly, M. *J. Biol. Chem.* **2003**, *278*, 45358–45367.
26. Aho, T. L.; Sandholm, J.; Peltola, K. J.; Mankonen, H. P.; Lilly, M.; Koskinen, P. J. *FEBS Lett.* **2004**, *571*, 43–49.
27. Laird, P. W.; van der Lugt, N. M.; Clarke, A.; Domen, J.; Linders, K.; McWhir, J.; Berns, A.; Hooper, M. *Nucleic Acids Res.* **1993**, *21*, 4750–4755.
28. Mikkers, H.; Nawijn, M.; Allen, J.; Brouwers, C.; Verhoeven, E.; Jonkers, J.; Berns, A. *Mol. Cell Biol.* **2004**, *24*, 6104–6115.
29. Lilly, M.; Sandholm, J.; Cooper, J. J.; Koskinen, P. J.; Kraft, A. *Oncogene* **1999**, *18*, 4022–4031.
30. Pircher, T. J.; Zhao, S.; Geiger, J. N.; Joneja, B.; Wojchowski, D. M. *Oncogene* **2000**, *19*, 3684–3692.
31. Lilly, M.; Kraft, A. *Cancer Res.* **1997**, *57*, 5348–5355.
32. Akasaka, H.; Akasaka, T.; Kurata, M.; Ueda, C.; Shimizu, A.; Uchiyama, T.; Ohno, H. *Cancer Res.* **2000**, *60*, 2335–2341.
33. Pasqualucci, L.; Neumeister, P.; Goossens, T.; Nanjangud, G.; Chaganti, R. S.; Kuppers, R.; Dalla-Favera, R. *Nature* **2001**, *412*, 341–346.
34. Dhanasekaran, S. M.; Barrette, T. R.; Ghosh, D.; Shah, R.; Varambally, S.; Kurachi, K.; Pienta, K. J.; Rubin, M. A.; Chinnaiyan, A. M. *Nature* **2001**, *412*, 822–826.
35. Valdmann, A.; Fang, X.; Pang, S. T.; Ekman, P.; Egevad, L. *Prostate* **2004**, *60*, 367–371.
36. Thaimattam, R.; Daga, P.; Rajjak, S. A.; Banerjee, R.; Iqbal, J. *Bioorg. Med. Chem.* **2004**, *12*, 6415–6425.
37. Sperandio da Silva, G. M.; Sant’Anna, C. M.; Barreiro, E. J. *Bioorg. Med. Chem.* **2004**, *12*, 3159–3166.
38. Ducrot, P.; Legerverend, M.; Grierson, D. S. *J. Med. Chem.* **2000**, *43*, 4098–4108.
39. Rieger, J. M.; Brown, M. L.; Sullivan, G. W.; Linden, J.; Macdonald, T. L. *J. Med. Chem.* **2001**, *44*, 531–539.
40. Peng, Y.; Keenan, S. M.; Zhang, Q.; Kholodovych, V.; Welsh, W. J. *J. Med. Chem.* **2005**, *48*, 1620–1629.
41. Kim, K. H.; Greco, G.; Novellino, E.; Silipo, C.; Vittoria, A. *J. Comput. Aided Mol. Des.* **1993**, *7*, 263–280.
42. Greco, G.; Novellino, E.; Fiorini, I.; Nacci, V.; Campiani, G.; Ciani, S. M.; Garofalo, A.; Bernasconi, P.; Mennini, T. *J. Med. Chem.* **1994**, *37*, 4100–4108.
43. Wong, G.; Koehler, K. F.; Skolnick, P.; Gu, Z. Q.; Ananthan, S.; Schonholzer, P.; Hunkeler, W.; Zhang, W.; Cook, J. M. *J. Med. Chem.* **1993**, *36*, 1820–1830.
44. Myers, A. M.; Charifson, P. S.; Owens, C. E.; Kula, N. S.; McPhail, A. T.; Baldessarini, R. J.; Booth, R. G.; Wyrick, S. D. *J. Med. Chem.* **1994**, *37*, 4109–4117.
45. Thomas, B. F.; Compton, D. R.; Martin, B. R.; Semus, S. F. *Mol. Pharmacol.* **1991**, *40*, 656–665.
46. Nordvall, G.; Hacksell, U. *J. Med. Chem.* **1993**, *36*, 967–976.
47. Agarwal, A.; Pearson, P. P.; Taylor, E. W.; Li, H. B.; Dahlgren, T.; Herslof, M.; Yang, Y.; Lambert, G.; Nelson, D. L.; Regan, J. W. *J. Med. Chem.* **1993**, *36*, 4006–4014.
48. Calder, J. A.; Wyatt, J. A.; Frenkel, D. A.; Casida, J. E. *J. Comput. Aided Mol. Des.* **1993**, *7*, 45–60.
49. Xing, L.; Welsh, W. J.; Tong, W.; Perkins, R.; Sheehan, D. M. *SAR QSAR Environ. Res.* **1999**, *10*, 215–237.
50. Mor, M.; Rivara, S.; Silva, C.; Bordi, F.; Plazzi, P. V.; Spadoni, G.; Diamantini, G.; Balsamini, C.; Tarzia, G.; Fraschini, F.; Lucini, V.; Nonno, R.; Stankov, B. M. *J. Med. Chem.* **1998**, *41*, 3831–3844.
51. Moro, S.; van Rhee, A. M.; Sanders, L. H.; Jacobson, K. A. *J. Med. Chem.* **1998**, *41*, 46–52.
52. Sicsic, S.; Serraz, I.; Andrieux, J.; Bremont, B.; Mathe-Allainmat, M.; Poncet, A.; Shen, S.; Langlois, M. *J. Med. Chem.* **1997**, *40*, 739–748.
53. Corelli, F.; Manetti, F.; Tafi, A.; Campiani, G.; Nacci, V.; Botta, M. *J. Med. Chem.* **1997**, *40*, 125–131.
54. Gantchev, T. G.; Ali, H.; van Lier, J. E. *J. Med. Chem.* **1994**, *37*, 4164–4176.
55. Chen, J. M.; Sheldon, A.; Pincus, M. R. *J. Biomol. Struct. Dyn.* **1993**, *10*, 1067–1089.
56. Haji-Momenian, S.; Rieger, J. M.; Macdonald, T. L.; Brown, M. L. *Bioorg. Med. Chem.* **2003**, *11*, 5545–5554.
57. Asikainen, A.; Tarhanen, J.; Poso, A.; Pasanen, M.; Alhava, E.; Juvonen, R. O. *Toxicol. In Vitro* **2003**, *17*, 449–455.
58. Ekins, S.; Bravi, G.; Wikel, J. H.; Wrighton, S. A. *J. Pharmacol. Exp. Ther.* **1999**, *291*, 424–433.
59. Ekins, S.; Bravi, G.; Ring, B. J.; Gillespie, T. A.; Gillespie, J. S.; Vandenbranden, M.; Wrighton, S. A.; Wikel, J. H. *J. Pharmacol. Exp. Ther.* **1999**, *288*, 21–29.
60. Jones, J. P.; He, M.; Trager, W. F.; Rettie, A. E. *Drug Metab. Dispos.* **1996**, *24*, 1–6.
61. Ma, X. H.; Zhang, X. Y.; Tan, J. J.; Chen, W. Z.; Wang, C. X. *Acta Pharmacol. Sin.* **2004**, *25*, 950–958.
62. Brown, M. L.; Rieger, J. M.; Macdonald, T. L. *Bioorg. Med. Chem.* **2000**, *8*, 1433–1441.
63. Holder, S.; Zemskova, M.; Zhang, C.; Tabrizizad, M.; Bremer, R.; Neidigh, J. W.; Lilly, M. B. *Mol. Cancer Ther.* **2007**, *6*, 163–172.
64. Clark, M. D.; Cramer, I. R. D.; Opdenbosch, N. V. *J. Comp. Chem.* **1989**, *10*, 982–1012.
65. Buolamwini, J. K.; Assefa, H. *J. Med. Chem.* **2002**, *45*, 841–852.
66. Chavatte, P.; Yous, S.; Marot, C.; Baurin, N.; Lesieur, D. *J. Med. Chem.* **2001**, *44*, 3223–3230.
67. Desiraju, G. R.; Gopalakrishnan, B.; Jetty, R. K.; Nagaraju, A.; Raveendra, D.; Sarma, J. A.; Sobhia, M. E.; Thilagavathi, R. *J. Med. Chem.* **2002**, *45*, 4847–4857.
68. Sippl, W. *J. Comput. Aided Mol. Des.* **2000**, *14*, 559–572.
69. Tammela, P.; Ekokoski, E.; Garcia-Horsman, A.; Talman, V.; Finel, M.; Tuominen, R.; Vuorela, P. *Drug Dev. Res.* **2004**, *63*, 76–87.
70. Jinsart, W.; Ternai, B.; Polya, G. M. *Biol. Chem. Hoppe-Seyler* **1992**, *373*, 205–211.
71. Austin, C. A.; Patel, S.; Ono, K.; Nakane, H.; Fisher, L. M. *Biochem. J.* **1992**, *282*(Pt 3), 883–889.
72. Hodnick, W. F.; Bohmont, C. W.; Capps, C.; Pardini, R. S. *Biochem. Pharmacol.* **1987**, *36*, 2873–2874.

73. Fesen, M. R.; Pommier, Y.; Leteurtre, F.; Hiroguchi, S.; Yung, J.; Kohn, K. W. *Biochem. Pharmacol.* **1994**, *48*, 595–608.
74. Robak, J.; Shridi, F.; Wolbis, M.; Krolikowska, M. *Pol. J. Pharmacol. Pharm.* **1988**, *40*, 451–458.
75. Murakami, S.; Muramatsu, M.; Tomisawa, K. *J. Enzyme Inhib.* **1999**, *14*, 151–166.
76. Ono, K.; Nakane, H.; Fukushima, M.; Chermann, J. C.; Barre-Sinoussi, F. *Eur. J. Biochem.* **1990**, *190*, 469–476.